OPEN ACCESS Freely available online

ISSN 2737-5323
Volume 4, Issue 2
https://afm.iikii.com.sg
Applied Functional Materials

Article

Growth of Chlorine-Doped ZnO Nanorod Arrays on Different Substrates

Tung-Lung Wu [1], Kao-Wei Min [2,] *, Ying-Tong Ye [3], Ming-Ta Yu [4], and Chi-Ting Ho [4]

[1] Department of Electrical Engineering, Lunghwa university of science and technology, Taoyuan, Taiwan; tunglung@mail.lhu.edu.tw
[2] Department of Electronic Engineering, Lunghwa university of science and technology, Taoyuan, Taiwan
[3] Department of Electronic Engineering, National Formosa University, Huwei, Yunlin 632, Taiwan; yumt@nfu.edu.tw
[4] Department of Mechanical Design Engineering, National Formosa University, Huwei, Yunlin 632, Taiwan; hoct@ms25.hinet.net
* Correspondence: el107@mail.lhu.edu.tw

Received: Apr 4, 2024; **Revised:** May 4, 2024; **Accepted:** May 8, 2024; **Published:** June 2, 2024

Abstract: In this study, zinc nitrate ($Zn(NO_3)_2$), hexamethylenetetramine ($C_6H_{12}N_4$), and sodium chloride (NaCl) were employed as precursor materials to synthesize ZnO nanorod arrays on two distinct types of substrates using the hydrothermal method. We investigated how different substrates and varying chlorine concentrations influence the synthesis properties of chlorine-doped ZnO nanorod arrays. Specifically, this study aimed to explore the structural, morphological, and optical properties of the synthesized ZnO nanorod arrays. The substrates investigated were an indium tin oxide (ITO) substrate with a ZnO seed layer and an ITO substrate with a self-assembled monolayer (SAM) of molecules. The formation of the SAM involved placing a clean ITO conductive glass substrate into a high-pressure reactor, along with a vial containing 0.2 mm of octadecyltrichlorosilane. Using this process, a uniform SAM was created on the ITO substrate. The molar ratio of $Zn(NO_3)_2$, $C_6H_{12}N_4$, and NaCl was maintained at 1:1:x, where x varied as 0, 0.1, 0.2, 0.3, and 0.4. This corresponded to NaCl volumes of 0, 2.5, 5.0, 7.5, and 10.0 mM, respectively. The crystallinity and orientation of the nanorods were assessed with their surface morphology using scanning electron microscopy (SEM). By systematically varying the chlorine concentration and substrate type, the role of these parameters was understood in tailoring the characteristics of ZnO nanorod arrays for potential applications in optoelectronic devices, sensors, and photocatalysts.

Keywords: Sodium chloride; Chlorine-doped ZnO nanorod arrays; Different substrates; Hydrothermal method

1. Introduction

Zinc oxide (ZnO) is garnering increasing attention due to its versatile properties as a one-dimensional (1-D) nanomaterial [1,2]. By employing various fabrication techniques, ZnO is fabricated in diverse nanostructures, each with distinct characteristics. Over the last decade, various ZnO nanostructures have been synthesized as nanorods, nanobelts, and nanoparticles. Among these, nanorods are particularly notable for their distinct and advantageous properties. Nanotechnology leverages the attributes of nanomaterials to construct structures in different dimensions. For instance, nanostructures such as quantum dots and wells are utilized for light-emitting or photodetecting capabilities. The interaction of light with such nanostructures significantly alters the light's properties, offering innovative applications in various fields. One-dimensional nanomaterials are pivotal for theoretical research in optical, electrical, magnetic, and mechanical properties and practical applications due to their excellent photoelectric and electronic characteristics. These properties make ZnO nanomaterials appropriate for developing nano-optoelectronic devices. Applications of ZnO nanomaterials include the following [3−5]: light-emitting diodes (LEDs), field emission devices, conductive material surface coatings, laser diodes (LDs), solar cells, gas sensors, photonic crystals, field-effect transistors (FETs), and photodetectors (PDs).

ZnO's properties as a piezoelectric semiconductor allow its use in thin-film form for surface acoustic wave (SAW) devices. Such a diverse range of applications underscores the immense potential of ZnO nanomaterials in improving various electronic and optoelectronic devices. ZnO is a notable II-VI group N-type wide bandgap semiconductor material known for its versatile properties and applications. Its crystal shows a symmetric hexagonal wurtzite structure. In this structure, each zinc atom is centrally located and tetrahedrally coordinated by four surrounding oxygen atoms, forming a dense hexagonal close-packed (HCP) configuration. The atomic layers are alternately arranged with zinc and oxygen planes along the C-axis, resulting in lattice constants of a=3.2495 Å and c=5.2069 Å with a C/A ratio of 1.633. ZnO is characterized by its high melting point of 1975°C and remarkable thermal stability at room temperature. It remains insoluble in alcohol and water but can be dissolved in alkalis and strong acids, indicating

its chemical resilience under various conditions. One of ZnO's most significant attributes is its wide direct bandgap of 3.37 eV at room temperature. This wide bandgap, combined with a high exciton binding energy of about 60 meV, surpasses that of other semiconductors with a high bandgap such as gallium nitride (GaN) which has an exciton binding energy of 25 meV. The substantial exciton binding energy of ZnO allows for a higher efficiency for light emission at room temperature. This property makes ZnO exceptionally appropriate for ultraviolet laser applications and short-wavelength optoelectronic devices. The combination of high thermal stability, chemical resilience, wide bandgap, and high exciton binding energy positions ZnO as a material with significant potential for advanced technological applications, particularly in the development of ultraviolet lasers, photodetectors, and other optoelectronic devices.

These characteristics highlight ZnO's pivotal role in advancing the performance and efficiency of next-generation optoelectronic systems. In the synthesis of ZnO nanomaterials, various methods are employed, each with unique advantages and applications. Vapor-phase methods for the synthesis of ZnO nanomaterials include the following.

1. Metal Organic Chemical Vapor Deposition (MOCVD): This method involves the chemical reaction of metal-organic compounds with a vapor-phase oxidant to deposit thin films of ZnO [6].
2. Pulse Laser Deposition (PLD): This technique uses high-power laser pulses to ablate a target material, which then deposits as a thin film on a substrate [7].
3. High-Temperature Furnace Chemical Vapor Deposition (CVD): This method uses high temperatures to facilitate chemical reactions in the vapor phase, leading to the deposition of ZnO [8].

For liquid-phase synthesis, the following methods are used.

1. Electrophoresis: This technique uses an electric field to move charged particles through a solution, depositing them on a substrate [9].
2. Template Method: This involves using a pre-formed template to guide the deposition and formation of ZnO nanostructures [10].
3. Hydrothermal Method: This process involves chemical reactions in aqueous solutions at elevated temperatures and pressures, leading to the growth of ZnO nanostructures [11].

In this study, the hydrothermal method was selected to grow ZnO nanorods based on its numerous benefits. This method operates at relatively low temperatures, is cost-effective, straightforward to implement, and produces high-quality ZnO with fewer defects and a higher success rate compared to other methods. For the synthesis, an initial aqueous solution was prepared by dissolving zinc nitrate ($Zn(NO_3)_2$), hexamethylenetetramine ($C_6H_{12}N_4$), and sodium chloride (NaCl) in deionized water in specific proportions. Using the hydrothermal method, chlorine-doped ZnO nanorod arrays were successfully grown on an indium tin oxide (ITO) substrate. The hydrothermal method's advantages, including its operational simplicity, low temperature, and high-quality output, make it a preferred choice for synthesizing ZnO nanorods. This approach is appropriate for applications requiring high-purity and defect-free nanostructures to mahufacture optoelectronic devices, sensors, and other advanced materials.

2. Materials and Methods

For the growth of ZnO nanorods, ITO transparent conductive glass was used as the primary substrate due to its favorable electrical and optical properties. The ITO glass had a thickness of 0.7 mm, and the thickness of an ITO film was 1800 Å. A sheet resistance was less than 10 Ω/sq, and the area was 37 × 40 cm^2. Before deposition, the glass was precisely cut into smaller dimensions of 1.5 × 3 cm^2 using a glass cutter. Ensuring the cleanliness of the substrate is critical for the successful adhesion and quality of the thin films. The cleaning process involves the following steps to eliminate contaminants and achieve a pristine substrate surface.

1. Acetone ultrasonic cleaning: The substrate is placed in a beaker filled with acetone (ACE), and an ultrasonic cleaner is used to sonicate the substrate for 10 min. This step effectively removes organic compounds and grease.
2. Isopropyl alcohol ultrasonic cleaning: The substrate is transferred to a beaker containing isopropyl alcohol (IPA) and sonicated for an additional 10 min to eliminate any residual acetone and organic contaminants.
3. De-ionized water (DI water) ultrasonic rinse: The substrate is placed in a beaker with DI water and sonicated for 10 min to wash away any remaining isopropyl alcohol.
4. Contamination inspection: The substrate surface is carefully inspected for any remaining contaminants. If contaminants are detected, the cleaning steps (1−3) are repeated until the substrate is thoroughly cleaned.
5. Drying with nitrogen: A nitrogen (N_2) gun is used to dry the substrate surface, ensuring no water droplets remain.
6. Oven drying: The substrate is placed in a 50°C oven and dried for one day to remove any residual moisture completely.

The ZnO nanorods were grown on two types of substrates: an ITO substrate with a ZnO seed layer and an ITO substrate with a self-assembled monolayer (SAM) of molecules. The growth process of the SAM involved placing a clean ITO conductive glass substrate into a high-pressure reactor with a vial containing 0.2 mm of octadecyltrichlorosilane. The reactor was then heated to 150°C and kept in an oven for 60 min to allow the substrate surface to form a self-assembled monolayer via thermal vapor deposition. By following the cleaning protocol, the substrate was prepared with a clean, contaminant-free surface for achieving high-quality ZnO nanorod growth and optimal film adhesion (Fig. 1). The liquid used to grow chlorine-doped ZnO nanorod arrays in this study was composed of zinc nitrate hexahydrate ($Zn(NO_3)_2$), hexamethylenetetramine (HMTA), and sodium chloride (NaCl) in a ratio of 1:1:x, where x ranged from 0 to 0.4. The liquid was kept in a hydrothermal solution for 12 h at 95°C. After the growth of ZnO nanorods, we employed scanning electron microscopy (FESEM) to examine the surface and cross-sectional morphologies of the synthesized ZnO nanorods. Energy dispersive X-ray spectroscopy (EDS) was integrated into the FESEM for elemental analysis.

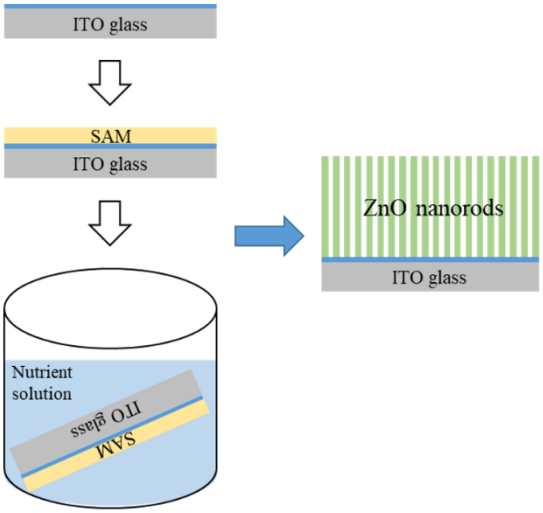

Fig. 1. Diagram of ZnO nanorods' fabrication process.

3. Results and Discussion

The FE-SEM images provided information on the structural and morphological characteristics of ZnO nanorods under different conditions and seed layers.

3.1. Uniform Deposition and Adhesion

Figure 2(a) shows the uniform and smooth deposition of ZnO films on ITO substrates, ensuring a consistent surface for subsequent nanorod growth. The side view highlights the excellent adhesion between the ZnO film and the ITO substrate, which is crucial for the stability of the nanorods (Fig. 2(b)).

3.2. Effect of Seed Layers on Nanorod Growth

3.2.1. ZnO Film as Seed Layer

Nanorods grown on the ZnO film were denser than those on the self-assembled monolayer (Figs. 3(a) and (b)). The ZnO film provides nucleation sites that promote the adherence and uniform growth of ZnO nanoparticles. The cross-sectional view shows vertically aligned nanorods with a height of about 2.2 μm, demonstrating the effectiveness of the ZnO film in directing vertical growth (Fig. 4(a)).

3.2.2. Self-assembled monolayers

Nanorods on self-assembled monolayers were less dense and taller with a height of approximately 9.4 μm (Fig. 4(b)). The reduced nucleation sites led to fewer but taller nanorods. The lack of a stabilizing seed layer causes the nanorods to tilt more easily, especially near fractured edges, indicating a less robust structure.

3.2.3. Impact of chlorine doping

Chlorine-doped ZnO nanorods exhibited improved growth patterns (Figs. 5(a) and (b)). The doping enhances the orderly and dense arrangement of nanorods, which contributes to chlorine's role in modifying the growth kinetics and surface energy of ZnO, leading to uniform and compact structures. These observations underscore the importance of seed layers and doping in controlling the morphology and growth characteristics of ZnO nanorods. The ZnO film seed layer and chlorine doping contribute to achieving desired structural properties, which are essential for various applications in optoelectronics and nanotechnology.

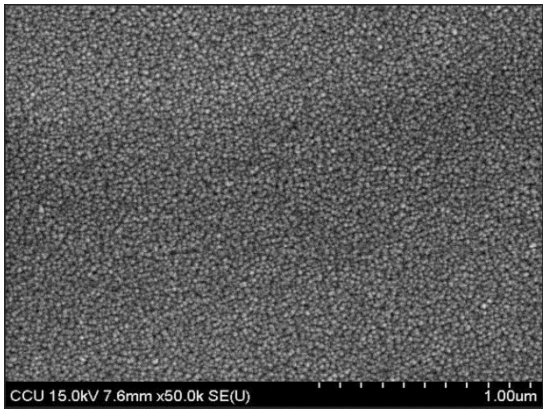

(**a**)

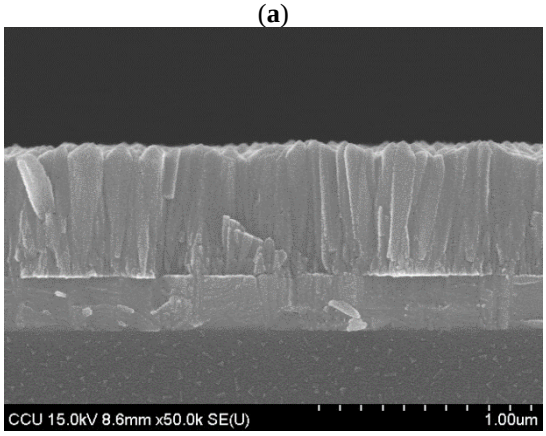

(**b**)

Fig. 2. ZnO seed layer (**a**) top view (**b**) cross-sectional view.

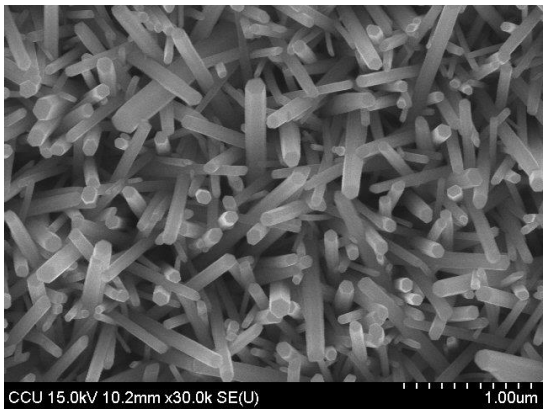

(**a**)

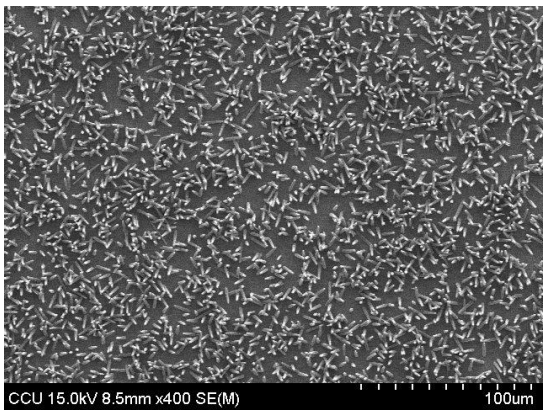

(**b**)

Fig. 3. Top observations of ZnO nanorods growth on (**a**) ZnO seed layer and (**b**) on self-assembled monolayer.

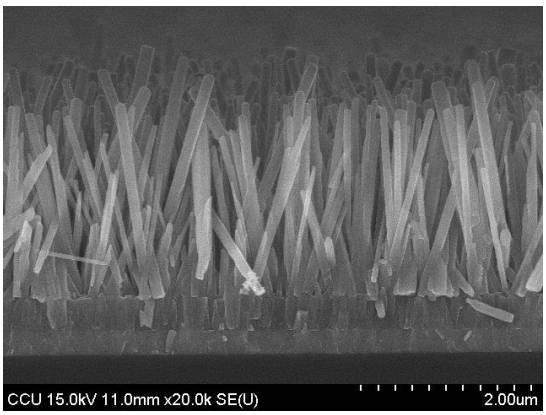

(**a**)

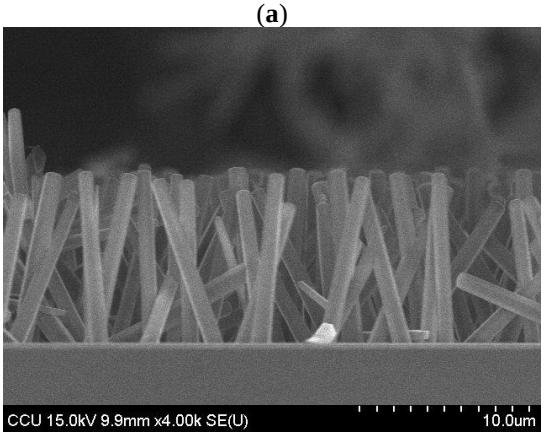

(**b**)

Fig. 4. Cross-sectional observations of ZnO nanorods growth on (**a**) ZnO seed layer and (**b**) on self-assembled monolayer.

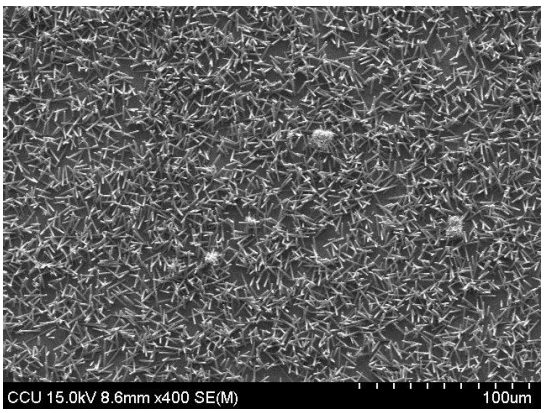

(a)

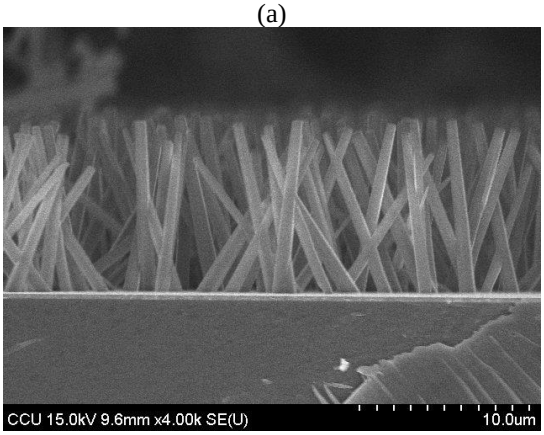

(b)

Fig. 5. ZnO nanorods growth on ZnO seed layer with 2.5 mM chlorine (a) top view (b) cross-sectional view.

The cross-sectional view reveals that the growth direction of chlorine-doped ZnO nanorods remains vertical to the substrate, with a column height of approximately 9.8 μm. Figures 6(a) and 6(b) illustrate ZnO nanorods doped with 5 mM chlorine. The top view shows that these nanorods are more upright, orderly, and densely packed compared to those doped with 2.5 mM chlorine, indicating a significant improvement in alignment and structural integrity. The cross-sectional view shows a notable increase in nanorod density, with a column height of approximately 10.4 μm. This enhanced vertical alignment and density suggest potential for applications requiring high surface area and uniformity. Figures 7(a) and 7(b) depict ZnO nanorods doped with 7.5 mM chlorine. The top view presents that these nanorods are even more upright, orderly, and densely packed than those doped with 5 mM chlorine. The increased doping concentration enhances the structural arrangement and packing density. The cross-sectional view shows that the nanorods grow longer, reaching a column height of approximately 11.6 μm. This suggests that higher chlorine doping promotes better alignment and growth, making these nanorods appropriate for applications requiring taller structures.

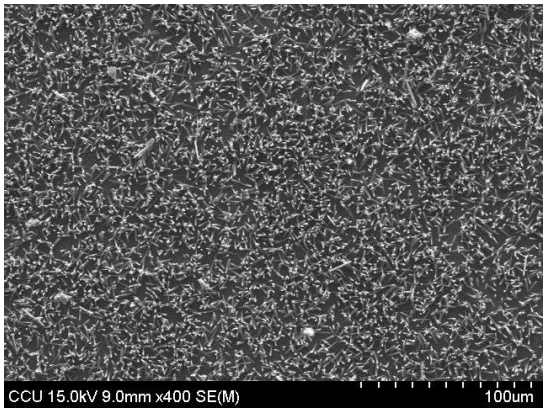

(**a**)

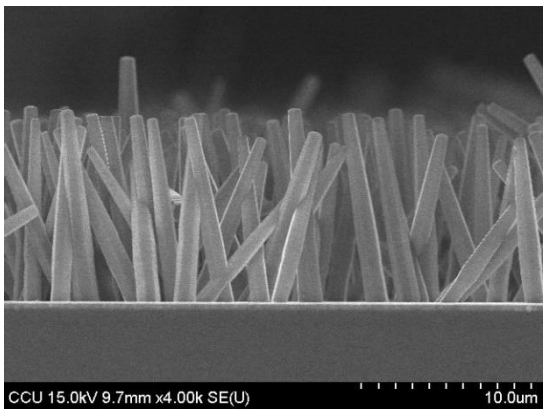

(**b**)

Fig. 6. ZnO nanorods growth on ZnO seed layer with 5 mM chlorine (**a**) top view (**b**) cross-sectional view.

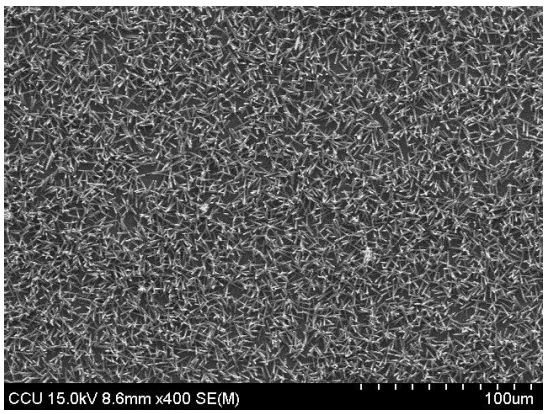

(**a**)

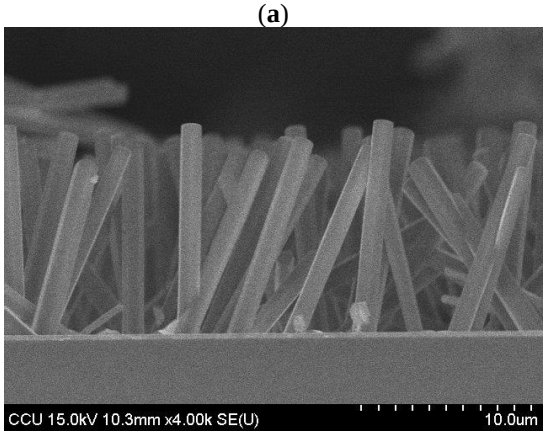

(**b**)

Fig. 7. ZnO nanorods growth on ZnO seed layer with 7.5 mM chlorine (**a**) top view (**b**) cross-sectional view.

Figures 8(a) and 8(b) present ZnO nanorods doped with 10 mM chlorine. The top view demonstrates that these nanorods achieve the highest density among all the doping concentrations, with an exceptional level of uprightness and order. The cross-sectional view shows that the nanorods grow longer, with a column height of approximately 12 μm. The increased length and density at this doping level indicate a superior structural framework, making these nanorods ideal for high-performance applications that demand the maximum surface area and optimal nanorod arrangement. The FE-SEM measurement results show that with increasing chlorine doping concentration, the ZnO nanorods grow more densely, uniformly, and vertically. The overall arrangement becomes orderly, and the width of the nanorods increases. The cross-sectional images demonstrate that higher chlorine doping concentrations enable uniform vertical growth and increased nanorod height. The results highlight the following effects of chlorine doping on ZnO nanorod growth.

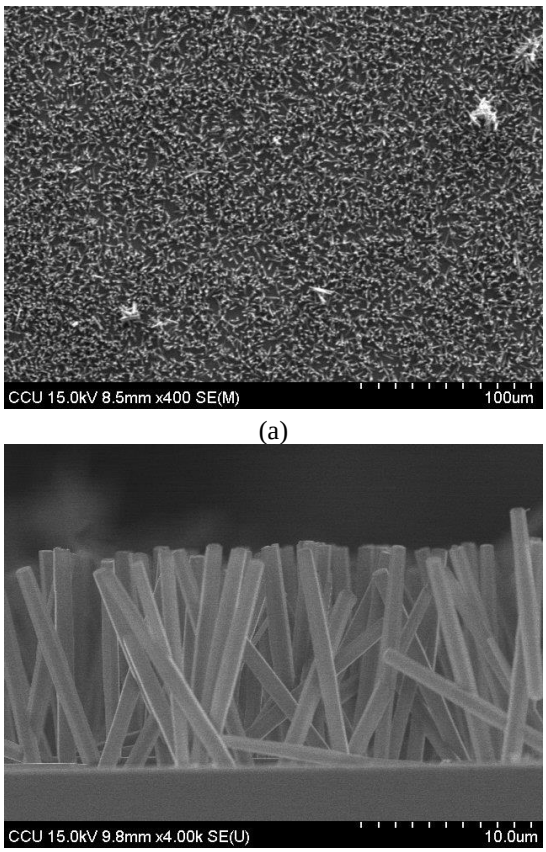

Fig. 8. ZnO nanorods growth on ZnO seed layer with 10 mM chlorine (**a**) top view (**b**) cross-sectional view.

1. Vertical growth and column height: In 2.5 mM chlorine doping, ZnO nanorods grow vertically with a height of approximately 9.8 μm. Increasing the chlorine concentration to 5 mM results in more upright and denser nanorods with a height of 10.4 μm. By increasing the concentration to 7.5 mM, the orderliness and density are enhanced, raising the column height to 11.6 μm. At 10 mM chlorine doping, the nanorods exhibit the highest density and a column height of approximately 12 μm.
2. Top view observations: The top views in Figs. 5 to 7 reveal a progressive increase in the alignment and density of the nanorods with higher chlorine doping. The nanorods become increasingly upright and well-ordered as the chlorine concentration increases from 2.5 mM to 10 mM.
3. Cross-sectional observations: The cross-sectional views show that higher chlorine doping concentrations lead to more densely packed nanorods. The vertical alignment and height of the nanorods improve significantly with increased doping concentrations, enhancing growth kinetics facilitated by chlorine doping.
4. Implications of chlorine doping: Chlorine doping significantly enhances the structural integrity and morphological characteristics of ZnO nanorods. Higher doping concentrations contribute to better vertical alignment and greater column heights, suggesting improved material properties for potential applications. The increased density and orderliness of the nanorods with higher doping concentrations improve their performance in optoelectronic devices, sensors, and other nanotechnology applications.
   These observations underscore the crucial role of chlorine doping in optimizing the growth and properties of ZnO nanorods, paving the way for their enhanced functionality in various technological applications.
5. The EDS images for ZnO nanorod arrays with chlorine of 0, 2.5, and 7.5 mM (Fig. 9) show that the proportion of the atomic weight of chlorine increases with higher doping concentrations. Specifically, the chlorine content is 0.24% for 2.5 mM, 0.27% for 5 mM (not shown here), 0.31% for 7.5 mM, and 0.79% for 10 mM (not shown here). The EDS results suggest that chlorine is successfully doped into the ZnO nanorods. The elemental distribution map confirms the chlorine incorporation in the ZnO nanorods. The distribution of chlorine observed in these maps corroborates the successful doping process and demonstrates a consistent presence of chlorine throughout the nanorod structure. Such results verify

the effect of chlorine doping which allows for the uniformity and effectiveness of the doping process. This is crucial for potential applications that rely on the modified properties of doped ZnO nanorods.

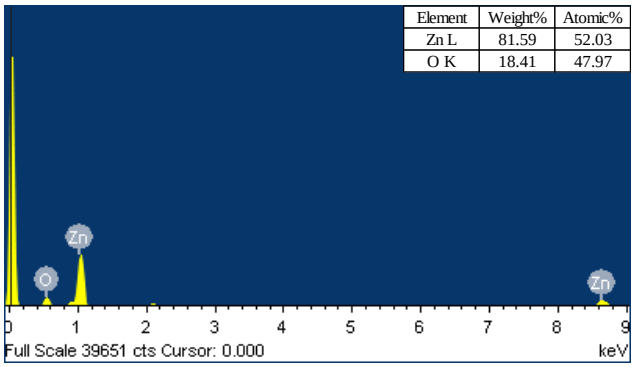

(a)

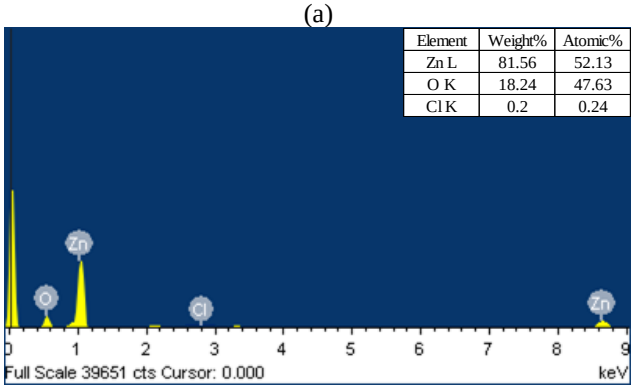

(b)

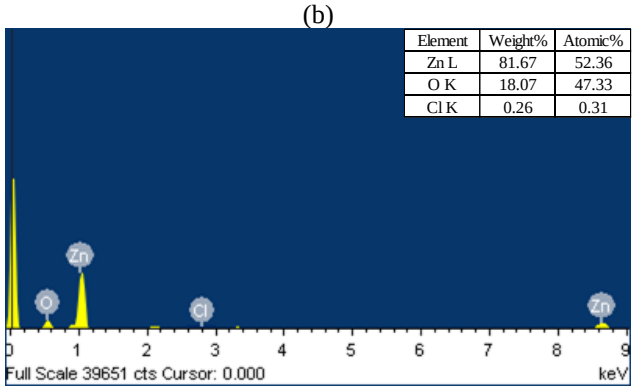

(c)

Fig. 9. Elemental analyses of (**a**) ZnO nanorods, (**b**) ZnO nanorods doped with 2.5 mM chlorine, and (**c**) ZnO nanorods doped with 7.5 mM chlorine.

4. Conclusions

The ZnO nanorods continue to grow longer and wider with an increase in chlorine doping. The increased density and orderliness of the nanorods with higher chlorine doping concentrations improve the performance of optoelectronic devices, sensors, and other nanotechnology devices using the nanorods. The EDS results suggested that chlorine is successfully doped into the ZnO nanorods and the concentration of chlorine observed in these maps increases and corroborates the successful doping process, demonstrating a consistent presence of chlorine in the nanorod structure.

Author Contributions: conceptualization, T.-L. Wu and Y.-T. Ye; methodology, M.-T. Yu and C.T. Ho; validation, Y.-T. Ye and K.-W. Min; formal analysis, T.-L. Wu and K.-W. Min; investigation, T.-L. Wu and Y.-T. Ye; resources, Y.-T. Ye; data curation, Y.-T. Ye and K.-W. Min; writing—original draft preparation, Y.-T. Ye; writing—review and editing, K.-W. Min; visualization, T.-L. Wu; supervision, M.-T. Yu and C.T. Ho. All authors have read and agreed to the published version of the manuscript.

Funding: This research received no external funding.

Data Availability Statement: Not applicable.

Conflicts of Interest: The authors declare no conflict of interest.

References

1. Wang, C.S.; Wang, F.H.; Liu, H.W. Growth of ZnO Nanoflower Arrays on a Patterned Sapphire Substrate. *Appl. Func. Mater.* **2021**, *1*, 54–59.
2. Yang, C.F.; Wang, C.S.; Wang, F.H.; Liu, H.W.; Micova, J. Effect of Synthesis Time on Synthesis and Photoluminescence Properties of ZnO Nanorods. *Appl. Func. Mater.* **2023**, *3*, 44–50.
3. Wang, Z.L.; Song, J. Piezoelectric Nanogenerators Based on Zinc Oxide Nanowire Arrays. *Science* **2006**, *312*, 242–246.
4. Wang, Z.L.; Chen, J.; Lin, L. Progress in triboelectric nanogenerators as a new energy technology and self-powered sensors. *Energy Environ. Sci.* **2015**, *8*, 2250–2282.
5. Wang, Z. L. Triboelectric nanogenerators as new energy technology for self-powered systems and as active mechanical and chemical sensors. *ACS nano*, **2013**, *7*, 9533–9557.
6. Tan, S.T.; Chen, B.J.; Sun, X.W.; Fan, W.J.; Kwok, H.S.; Zhang, X.H.; Chua, S.J. Blueshift of optical band gap in ZnO thin films grown by metal-organic chemical-vapor deposition. *J. Appl. Phys.* 2005, *98*, 013505.
7. Sun, X.W.; Kwok, H.S. Optical properties of epitaxially grown zinc oxide films on sapphire by pulsed laser deposition. *J. Appl. Phys.* **1999**, *86*, 408–411.
8. Wu, J.J.; Liu, S.C. Low-temperature growth of well-aligned ZnO nanorods by chemical vapor deposition. *Adv. Materi.* **2002**, *14*, 215–218.
9. He, H.; Cai, W.; Lin, Y.; Chen, B. Surface decoration of ZnO nanorod arrays by electrophoresis in the Au colloidal solution prepared by laser ablation in water. *Langmuir* **2010**, *26*, 8925–8932.
10. Fan, H.J.; Lee, W.; Hauschild, R.; Alexe, M.; et al. Template-assisted large-scale ordered arrays of ZnO pillars for optical and piezoelectric applications. *Small* **2006**, *2*, 561–568.
11. Tam, K.H.; Cheung, C.K.; Leung, Y.H.; Djurišić, A.B.; et al. Defects in ZnO nanorods prepared by a hydrothermal method. *J. Phys. Chem. B*, **2006**, *110*, 20865–20871.

Publisher's Note: IIKII stays neutral with regard to jurisdictional claims in published maps and institutional affiliations.